Preparation of A Layered Aurivillius– Perovskite Oxide as a Photocatalyst for Removal of Azo Dye from Industrial Wastewaters under Visible- Light Irradiation

Niyazi A. S. Al-Areqi[1],Sameh A. S. Alariqi[2], Amin Albirihi[3], Etehad Fisal[1, *]

Abstract—A layered Aurivillius–perovskite type BINIVOX system with the general formula, $Bi_2Ni_xV_{1-x}O_{5.5-(3x/2)}$ was developed as a novel photocatalyst for degradation of organic dyes. A series of BINIVOX.x catalysts in the composition range $0 \le x \le 0.20$ were successfully synthesized by the standard solid– state reaction and characterized using X–ray powder diffraction (XRD), differential thermal analysis (DTA), UV–vis absorption spectroscopy and BET surface area. Then, the photocatalytic activities of prepared catalysts were investigated for the first time through the degradation of a new azo dye, namely SDN in aqueous solution under visible light irradiation. Adsorption efficiency and photocatalytic activity of BINIVOX.*x* catalysts were correlated well with the variation in phase crystal structures stabilized at room temperature as a function of composition. The stabilized β–BINIVOX phases in the orthorhombic crystal system with space group Acam exhibited the best photocatalytic performance which can be attributed to their higher specific surface area, narrower band– gap energy, higher oxygen –vacancy concentration in the perovskite vanadate layers. In addition, the possible photocatalytic degradation mechanism of aqueous SDN dye was proposed under visible light irradiation.

Index Terms— Photocatalyst, BINIVOX, SDN, Perovskite, Oxide.

1 INTRODUCTION

SYNTHETIC dyes comprise an important part of industrial wastewaters, as they are discharged in abundance by many manufacturing industries. The impact of these dyes on the environment is a major concern because of the potentially carcinogenic properties of these chemicals [1]. Besides this, some dyes can undergo anaerobic decoloration to form potential carcinogens [2,3]. The wastewaters which are colored in the presence of these dyes can block both sunlight penetration and oxygen dissolution, which are essential for aquatic life. Many researches have been devoted in the literature to develop typical techniques for removal of pollutant dyes from industrial wastewaters, particularly azo dyes constituting the majority of use [4–10]. All these classical techniques are versatile and useful, but they all end up in producing a secondary waste product which needs to be processed further. Another set of techniques which are relatively newer, more powerful, and very promising is called Advanced Oxidation Processes (AOPs) which has been developed and employed to treat dye-contaminated wastewater effluents [11,12]. This methodology would normally utilize a strong oxidizing species such as •OH radicals produced in situ, which causes a sequence of reactions thereafter to break down the macromolecules like dyes into smaller and less harmful substances. The AOP technique has drawn considerable attention from various quarters of scientific community as it is easy to handle and produces significantly less residuals as compared to the classical approaches. Many metal oxides such as TiO_2 , ZnO, ZrO_2 etc. have been widely investigated in the AOPs for the photodegradation of synthetic dyes in wastewater. However, because of their relatively high band–gap energy, they are activated only by ultraviolet light absorption [13–15], which limits their commercial application for water and wastewater treatment. To overcome this problem, the visible light induced photocatalysts are required to apply the AOPs more feasible and to degrade these dyes using the viable energy of sunlight.

In our previous work on the electrical properties of oxide– ion conductors, *viz.* BIMEVOX (Bi= bismuth, Me= dopant metal ion, V= vanadium, and OX= oxide) derived by the partial substitution of Me for V in the parent compound, $Bi_2VO_{5.5}$ of a layered Aurivillius–type structure, It has been found that many of BIMEVOX materials possess colors and behave as semiconductors at temperatures lower than 300 °C [16–18].

BIMEVOX ($Bi_2Me^l_xV_{1-x}O_{5.5-(5-l)x/2}$) can be described as $(Bi_2O_2)^{2+}$ layers alternating with $(VO_{3.5}\square_{0.5})^{2-}$ /($Me^l_xV_{1-x}O_{3.5-(5-l)x/2}\square_{0.5})^{2-}$ perovskite–like slabs, where l and $\square$ stand for the valence of a metal dopant and oxygen vacancy, respectively. Depending on the concentration of a metal dopant the BIMEVOX can exist in three essential phases; α (monoclinic), β (orthorhombic) and the γ (tetragonal)–phases at room temperature [19, 20]. So the present work aims to investigate the catalytic efficiency of the BINIVOX system, $Bi_2Ni_xV_{1-x}O_{5.5-(3x/2)}$ for the visible -light photodegradation of a new synthesized azo dye, Sodium 4–[(*E*)–(4,5–dimethyl–1*H*–pyrazolo [3,4–*c*] pyridazin–3–yl) diazenyl] naphthalen–1–olate ($C_{17}H_{13}N_6ONa$,

- [1] *Department of Chemistry, Faculty of Applied Science, Taiz University, Taiz Yemen, Corresponding authoe E-mail:niyazi75.alareqi@gmail.com* (N.S.A. Al-Areqi), *Etehad7714@gmail.com (E. Faisal).*
- [2] *Department of Industrial Chemistry, Faculty of Applied Science, Taiz University, Taiz Yemen*
- [3]*Ministry of Education, Sana'a, Yemen*

340.315 g mol^{-1}), which was abbreviated as SDN in the following context for the sake of simplicity.

2 Materials & Methods

2.1 Catalyst preparation

A layered Aurivillius–perovskite type BINIVOX.x photocatalysts of the general formula, $Bi_2Ni_xV_{1-x}O_{5.5-(3x/2)}$; $0.0 \le x \le 0.20$, was synthesized by the standard solid–state reaction. Appropriate amounts of Bi_2O_3 (Aldrich, 99.9%), V_2O_5 (ABCR, 99.5%), NiO (Aldrich, 99.5%) were ground together as a (1:1) acetone–toluene paste, according to the reaction equation:

$$Bi_2O_3 + \frac{(1-x)}{2} V_2O_5 + x\ NiO \rightarrow Bi_2Ni_x^{(II)}V_{1-x}O_{5.5-(3x/2)} \quad (1)$$

The resulting pastes were calcined in a muffle furnace at 650 ^oC for 20 hours. At the end of reaction, the product was slowly quenched in air to room temperature. The same procedure was repeated several times with intermediate grindings in acetone– toluene solvent to ensure the completion of reaction.

2.2 Photocatalyst characterization

The X–ray powder diffraction (XRD) patterns obtained on a Philips PW 1050/30 X–ray diffractometer using CuK_α radiation (λ=1.54060 Å), were used to determine the identity of stabilized phases present and their crystallite sizes. The diffraction beams were collected using the Bragg–Brentano geometry in the range of $10^o \le 2\theta \le 90^o$ with an increment of 0.15^o at scantime of 1.3 sec/increment. The unit cell parameters were refined using a *POWDERX* software program. The average crystallite size was calculated from the diffraction line broadening via the Scherrer equation:

$$D = \frac{0.89\lambda}{B\cos\theta} \quad (2)$$

where D is the crystal size in nm, λ is the CuK_α radiation wavelength (λ=1.54060Å), B is the half–width of the peak in radians and θ is the corresponding diffraction angle.

Differential thermal analysis (DTA) thermograms collected on a Perkin–Elmer thermal analyzer, were used to investigate the thermal stability range of different phases of the catalyst. Approximately weighed 20–mg dry samples of BINIVOX photocatalysts were placed in α–alumina cell. The experiments were run in N_2 atmosphere. The flow rate of N_2 was maintained at 30 ml min^{-1} with a heating rate of 10 ^oC min^{-1} from ambient to 1000 ^oC.

The optical band–gap energies (E_g) for the photocatalysts was estimated from UV–vis absorption spectra , collected on a Shimadzu Scan UV–vis spectrophotometer (UV–2450) at room temperature in the wavelength range 200–800 nm. The direct band– gap energy was calculated from the wavelength corresponding to the band–gap edge absorption(λ_g) using Eq.(3):

$$E_g(eV) = \frac{1240}{\lambda_g(nm)} \quad (3)$$

Surface area measurements were performed by nitrogen adsorption– desorption isotherm at 77 K on an Autosorb–1(Quantachrome) adsorption apparatus. The adsorption data were collected in the nitrogen partial pressure (P/P_o) range of 0.01–0.99. The specific surface areas (S_{BET}) expressed in m^2/g, were calculated by Brunauer–Emmett–Teller method.

2.3 Photocatalytic activity measurements

A 250–ml aqueous solution of 5×10^{-4} M SDN dye solution at pH ~10.0 (adjusted with diluted aqueous solution of NH_3 and H_2SO_4) was placed in a 450 ml – photoreactor equipped with a magnetic stirrer. Before photocatalytic reaction, 200–mg powdered sample of the photocatayst was dispersed in the dye aqueous solution. The resulting suspension was then magnetically stirred in the dark for 25 min to reach the adsorption–desorption equilibrium. The visible light with wavelengths greater than 400 nm using a 300–W Xe lamp was irradiated perpendicularly to the surface of solution at affixed distance between the visible source and the surface of dye solution (25 cm). At specific time intervals (10 min) about 5ml– aliquot of the reaction mixture was withdrawn from the photoreactor and then filtered to separate the catalyst residues. The concentrations of dye versus irradiation time were determined by measuring the maximum absorbance (λ_{max}= 525nm) using a Shimadzu UV–vis spectrophotometer (UV–1240). The photocatalytic activity of the BINIVOX.x catalyst as a function of composition for the dye photodegradation was investigated using a pseudo first–order kinetic model.

$$ln(C_t / C_o) = -k_{app}\ t \quad (4)$$

where C_o and C_t are the initial concentration and concentration at time, t of SDN dye solution, respectively and k_{app} denotes the apparent first–order rate constant.

3 Results and Discussion

3.1 X–ray crystallography

The variation in XRD patterns of as–synthesized BINIVOX.x photocatalysts as a function of Ni substitution is illustrated in Fig. 1. The diffraction patterns for the catalyst compositions x < 0.10 appear to be identical to the characteristic α–phase diffraction pattern observed for $Bi_4V_2O_{11}$, indicating no significant polymorphism occurs in the substituted system with increasing Ni content upto x < 0.10. However, the stabilization of β–BINIVOX.10 phase is clearly evidenced by the existence of doublet sublattice peak (020) and (200) at 2θ ~ 32^o,and singlet peak (220) at 2θ ~ 46.2^o which are characteristic to the orthorhombic symmetry with a space group, *Acam* [21]. the low–temperature tetragonal γ'–BINIVOX.13 phase in space group, *I4/m mm* is stabilized, which is definitely clear from the ap-

pearance of a singlet sublattice peak indexed as (110) at 2θ ~ 32° [22].

Values of unit cell refinement, average crystallite size and crystallographic density obtained from fitting diffraction patterns are listed in Table 2. It is clear that the substitution of Ni into the $Bi_4V_2O_{11}$ compound causes a dramatic increase in the unit cell dimensions (particularly *a* and *c*), accompanied by the same trend in the overall cell volume. The density strongly depends on the initial crystallite size. The density and particle size are both lowered slightly with the increase of Ni dopant content. This trend is in a good agreement with the variation of unit cell parameters, reflecting the positive contribution of Ni substitution to the overall lattice expansion as a result of the incorporation of Ni(II) dopant ions of larger ionic radius (0.83 Å) into the perovskite vanadate layers in the place of pentavalent vanadium sites (0.54 Å)[23].

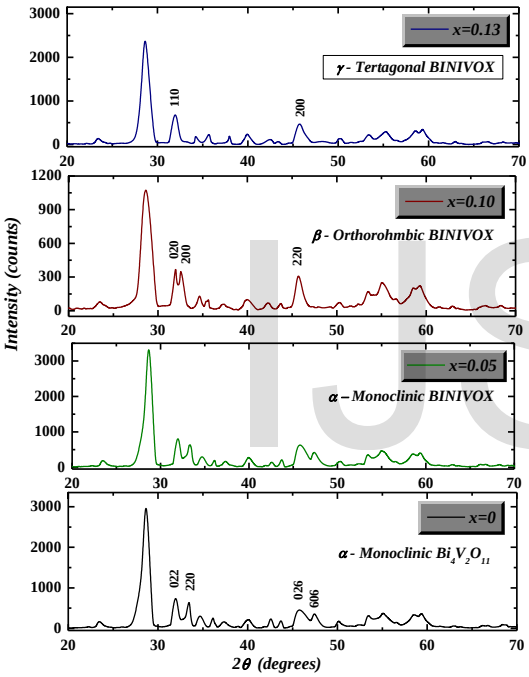

Fig. 1. XRD patterns of as–synthesized BINIVOX.*x* photocatalysts.

3.2 Thermal Analysis

Thermal stability of the BINIVOX.*x* system and the onset temperature of phase transition are presented in the DTA thermograms (Fig. 2). The two characteristic endothermic peaks clearly seen for the BINIVOX.05 photocatalyst are attributed to the consequent α→β and β→γ transitions [24,25]. It can also be observed that the heat flow per unit mass of the α→β transition is nearly three orders of magnitude higher than that of the β→γ transition. However, the β–BINIVOX.10 photocatalyst shows a single endothermic peak 464.2 °C assigned to the β→γ transition, while the occurrence of incommensurate → commensurate, γ'→γ transition is detected for γ'–BINIVOX.13 photocatalyst [26,27].

3.3 Optical and surface properties

Fig. 3 shows UV–vis absorption spectra of the BINIVOX.*x* system for various compositions. The pure $Bi_4V_2O_{11}$ displays a typical absorption in the visible region of spectrum with an absorption edge of ~ 593 nm, which is assigned to the intrinsic band– gap absorption of $Bi_4V_2O_{11}$ due to the electronic transitions from *Bi6s*/*O2p* orbitals of the bismuthate $(Bi_2O_2)^{2+}$ layers (valence band) to the conduction band consisting of *V3d* orbitals of the $(VO_{3.5}\square_{0.5})^{2-}$ perovskite–like slabs [12]. The absorption edges of the BINIVOX.*x* photocatalysts are found to shift toward longer wavelengths as the dopant concentration increases. This trend is quite consistent with the additional contribution of *Ni3d* orbitals to the conduction band [28] and increasing oxygen vacancy concentration [24] in the perovskite vanadate layers. The influence of Ni substitution on the optical band–gap energy of the BINIVOX.*x* system is illustrated in Table 2.

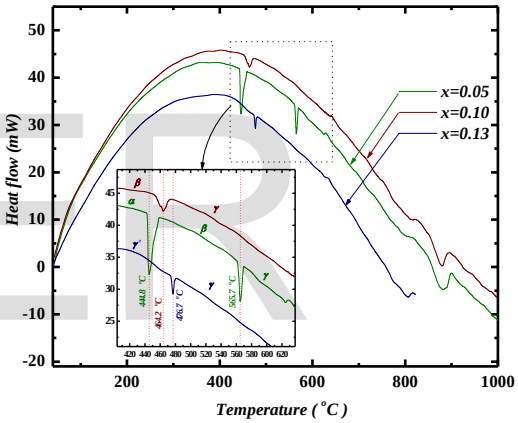

Fig. 2. DTA thermograms of as–synthesized BINIVOX.*x* photocatalysts.

It is confirmed that the band–gap energy tends to be narrower with increasing Ni content, suggesting that the aliovalent transition metal doping strategy plays a significant role in improving the photoabsorption and photocatalytic activities of $Bi_4V_2O_{11}$.The decreased band–gap energy are found to match well with the increase in the corresponding special surface areas (S_{BET}) as shown in Table 1. This preliminary trend is basically due to the increase of active sites available on the conduction band, *i.e.* the positively charged oxygen vacancies created at the equatorial planes of perovskite vanadate layers as a result of increasing Ni substitution [29-31]. The interesting point to be emphasized here is that the SDN dye molecules are expected to adsorb onto the perovskite vanadate layers and this adsorption is effectively enhanced by the coulombic interaction between negatively charged oxygen atoms of the dye and equatorial oxygen vacancies available on the conduction band (CB), suggesting that the BINIVOX.*x* photocatalysts with

TABLE 1
REFINED UNIT CELL PARAMETERS, CRYSTALLOGRAPHIC DENSITIES, AVERAGE CRYSTALLITE SIZES AND SPECIFIC SURFACE AREAS OF AS–PREPARED BINIVOX.*x* PHOTOCATALYST SERIES.

x	*Unit cell parameters*				d_{XRD} (g cm^{-3})	*Average Crystallite size* (μm)	*BET surface area* (m^2/g)
	a(Å)	*b*(Å)	*c* (Å)	*V*(Å^3)			
0.00	5.521	5.627	15.293	475.10	6.78	4.12	0.21
0.05	5.544	5.617	15.355	478.17	6.56	4.04	0.27
0.10	5.624	5.621	15.393	486.61	6.47	3.86	0.31
0.13	5.629	–	15.398	487.90	6.43	3.81	0.37

layered Aurivillius– perovskite type structures can offer high specific surface areas and more active sites available for dye adsorption and consequently favorable for enhancing photocatalytic performance.

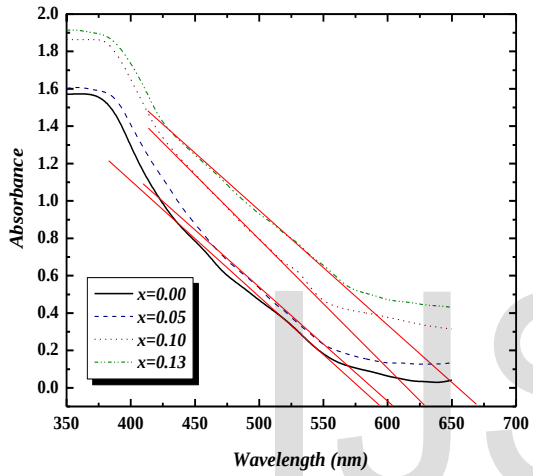

Fig. 3. UV–vis spectra of the BINIVOX.*x* photocatalysts

TABLE 2
VALUES OF BAND- GAP ENERGY FOR THE BINIVOX.*x* PHOTOCATALYSTS

x	λ_{ab}(nm)	E_g (eV)	*SD*	*R*-
0.00	593.34	2.09	0.0241	0.9847
0.05	603.67	2.05	0.0182	0.9863
0.10	628.65	1.97	0.0144	0.9887
0.13	670.85	1.85	0.0098	0.9898

3.4 Photocatalytic activity and mechanism

The photocatalytic degradation efficiency of SDN dye with varying BINIVOX.*x* catalyst compositions is presented in Fig. 4. It is observed that the degradation rate in the presence of equally weighted amounts of BINIVOX.*x* photocatalysts initially increases with increasing Ni dopant content upto *x*=0.10 and thereafter it sharply decreases for the BINIVOX.13-photocatalyzed reaction. It is interesting to note that the photodegradation of SDN dye proceeds more slowly when catalyzed by the BINIVOX.*x* system whose Ni content lies in the compositional range of the γ′–phase stabilization.

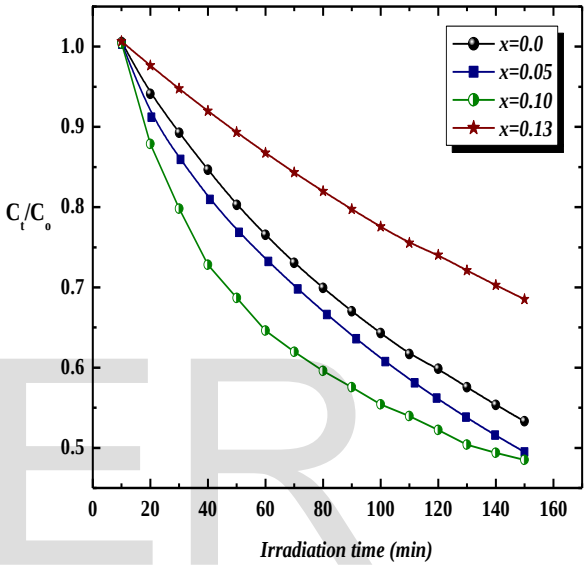

Fig. 4. Photocatalytic activities of the BINIVOX.*x* catalyst series for the degradation of SDN dye solution under visible light irradiation.

The values of k_{app} (min^{-1}) were calculated from the slopes using the line–regression fitting to the first– order kinetic model as shown in Fig. 5. The variation of k_{app} as a function of the photocatalyst composition and corresponding regression determination coefficients (*R*) are illustrated in Table 3.

The maximum value of k_{app} for the BINIVOX.10 photocatalyst suggests that the visible light photocatalytic activity of the β–BINIVOX.*x* catalyst is greatly enhanced by the oxygen–vacancy creation at equatorial planes of the perovskite vanadate layers [29]. However, the lowering in the photocatalytic degradation rate of the dye with stabilized γ′– photocatalyst phases is attributed to the increasing apical vacancies that may enhance the recombination of photo–induced holes and electrons and thereby reducing the visible light photocatalytic activity of the BINIVOX.*x* system.

The photocatalytic mechanism of SDN dye degradation using the BINIVOX.*x* catalyst under visible light irradiation is suggested in Fig. 6. Initially, the nickel doping narrows the band gap of the photocatalysts to enhance visible light absorption [32]. The SDN dye molecules are then adsorbed onto the perovskite vanadate layers as a result of a coulombic interaction

between negatively charged oxygen atoms of the dye and equatorial oxygen vacancies available on the conduction band (CB). Under irradiated visible light energy , The mechanism suggests that excitation of the adsorbed SDN dye takes place by visible light absorption to the appropriate singlet or triplet states, subsequently followed by electron ejection from the excited dye molecule onto the conduction band, while the dye is converted into a cationic dye radical($SDN^{\cdot+}$) that undergoes degradation to yield mineralization products.

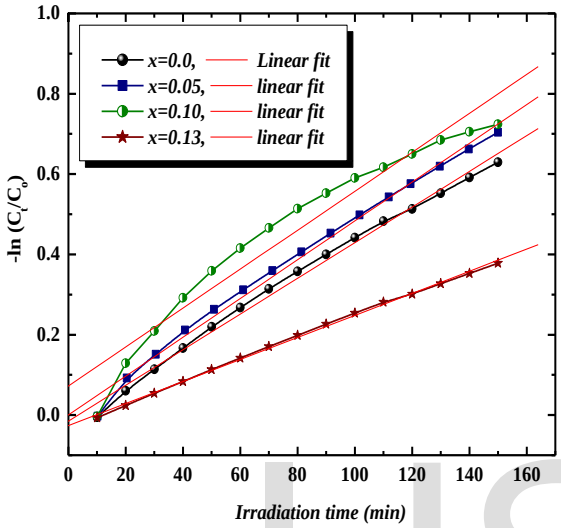

Fig. 5. Linear least– squares fitted plots of ln(C/Co) versus irradiation time of the pseudo first–order kinetics for the visible– light photodegradation of SDN dye catalyzed by various compositions of the BINIVOX.x system.

TABLE 3
VARIATION IN THE RATE CONSTANT OF PHOTOCATALYTIC DEGRADATION OF SDN DYE AS A FUNCTION OF NI SUBSTITUTION IN BINIVOX CATALYST.

x	k_{app} (min^{-1}) × 10^{-3}	SD	R
0.00	4.44	0.0171	0.9966
0.05	4.83	0.0192	0.9963
0.10	4.85	0.0552	0.9712
0.13	2.75	0.0052	0.9992

The photocatalytic mechanism of SDN dye degradation using the BINIVOX.x catalyst under visible light irradiation is suggested in Fig. 6. Initially, the nickel doping narrows the band gap of the photocatalysts to enhance visible light absorption [32]. The SDN dye molecules are then adsorbed onto the perovskite vanadate layers as a result of a coulombic interaction between negatively charged oxygen atoms of the dye and equatorial oxygen vacancies available on the conduction band (CB). Under irradiated visible light energy , The mechanism suggests that excitation of the adsorbed SDN dye takes place by visible light absorption to the appropriate singlet or triplet states, subsequently followed by electron ejection from the excited dye molecule onto the conduction band, while the dye is converted into a cationic dye radical($SDN^{\cdot+}$) that undergoes degradation to yield mineralization products.

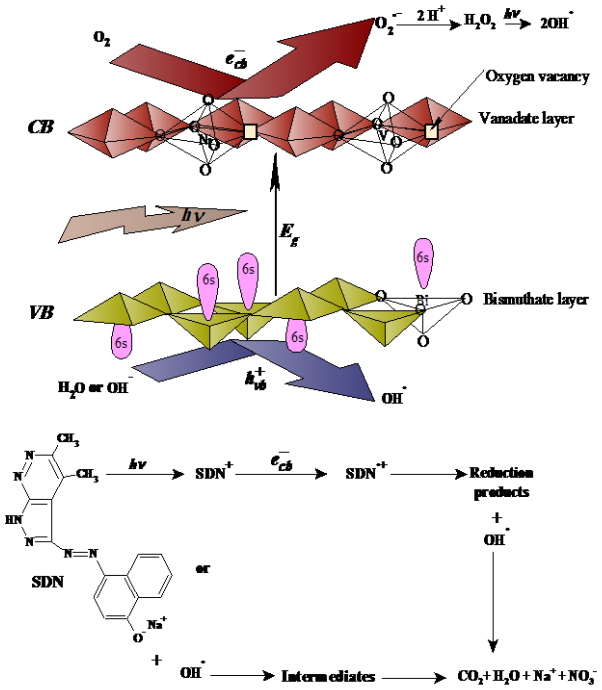

Fig. 6. Proposed mechanism of the SDN dye degradation by the BI-NIVOX.x photocatalysts under visible light irradiation.

4 CONCLUSION

In presented study, a ternary–metal oxide with Aurivillius–type structure, viz. BINIVOX.x system, has been developed as a photocatalyst for dyes degradation under visible light irradiation. It has been found that the partial substitution of V(V) in α– $Bi_4V_2O_{11}$compound by Ni(II) leads to the stabilization of photocatalytically active β–phases exhibiting the higher efficiency for the electron–hole generation and the lower recombination rate of the electron–hole. The superior photocatalytic activity of this stabilized β–phase were ascribed to its higher specific surface area, narrower band– gap energy, higher oxygen –vacancy concentration in the perovskite– vanadate layers. Accordingly, These last interesting features confers to the stabilized β–BINIVOX system an efficient photocatalyst for the degradation of anionic azo dyes.

ACKNOWLEDGMENTS

The authors are grateful to Prof. Saba Beg, Department of Chemistry, Aligarh Muslim University, Aligarh- India for providing research facilities and her fruitful discussion.

REFERENCES

[1] S. Parsons, Advanced Oxidation Processes for Water and Wastewater, IWA Publishing, London, UK, 2004. (references)

[2] M. Zubair Alam, S. Ahmad, A. Malik, M. Ahmad, Mutagenicity and genotoxicity of tannery effluents used for irrigation at Kanpur, India, *Ecotoxicology and Environmental Safety* 73 (2010) 1620–1628.

[3] C. O'Neill, A. Lopez, S. Esteves, F.R. Hawkes, D.L. Hawkes, S. Wilcox, Azo-dye degradation in an anaerobic-aerobic treatment system operating on simulated textile effluent, *Applied Microbiology and Biotechnology* 53 (1999) 249–254.

[4] N. Nasuha, B.H. Hameed, A.T.M. Din, Rejected tea as a potential low-cost adsorbent for the removal of methylene blue, *Journal of Hazardous Materials* 175 (2010) 126–132.

[5] M.J. Martin, A. Artola, M.D. Balaguer, M. Rigola, Activated carbons developed from surplus sewage sludge for the removal of dyes from dilute aqueous solutions, *Chemical Engineering Journal* 94 (2003) 231–239.

[6] M.A. Rauf, S.M. Qadri, S. Ashraf, K.M. Al-Mansoori, Adsorption studies of Toluidine Blue from aqueous solutions onto gypsum, *Chemical Engineering Journal* 150 (2009) 90–95.

[7] A.L. Ahmad, S.W. Puasa, Reactive dyes decolourization from an aqueous solution by combined coagulation/micellar-enhanced ultrafiltration process, *Chemical Engineering Journal* 132 (2007) 257–265.

[8] M. Riera-Torres, C. Gutiérrez-Bouzán, M. Crespi, Combination of coagulation flocculation and nanofiltration techniques for dye removal and water reuse in textile effluents, *Desalination* 252 (2010) 53–59.

[9] K. Shakir, A.F. Elkafrawy, H.F. Ghoneimy, S.G. Elrab Beheir, M. Refaat, Removal of rhodamine B (a basic dye) and thoron (an acidic dye) fromdilute aqueous solutions and wastewater simulants by ion flotation, *Water Research* 44 (2010) 1449–1461.

[10] S. Zodi, O. Potier, F. Lapicque, J.-P. Leclerc, Treatment of the industrial wastewaters by electrocoagulation: optimization of coupled electrochemical and sedimentation processes, *Desalination* 261 (2010) 186–190.

[11] M.A. Rauf, S.S. Ashraf, Application of Advanced Oxidation Processes (AOP) to dye degradation—an overview, in: Arnold R. Lang (Ed.), Dyes and Pigments: New Research, Nova Science Publishers, Inc, 2009.

[12] M. Pera-Titus, V. García-Molina, M.A. Baños, J. Giménez, S. Esplugas, Degradation of chlorophenols by means of advanced oxidation processes: a general review, *Applied Catalysis B: Environmental* 47 (2004) 219–256.

[13] O. Legrini, E. Oliveros, A.M. Braun, Photochemical processes for water treatment, Chemical Review 93 (1993) 671–698.

[14] I.K. Konstantinou, and T.A. Albanis, TiO_2–assisted photocatalytic degradation of azo dyes in aqueous solution: Kinetic and mechanistic investigations: A review, *Applied Catalysis B: Environmental* 49 (2004) 1–14.

[15] A. D. Paola, E. García–López, G. Marcì, and L. Palmisano A survey of photocatalytic materials for environmental remediation, *Journal of Hazardous Materials* 211– 212 (2012) 3– 29.

[16] N. A.S. Al–Areqi, S. Beg, Studies in composition and temperature dependence of phase stability in the $Bi_4Ag_xV_{2-x}O_{11-\ (2x/)-\delta}$ system and their influence on the oxide ion performance, *Phase Transitions* 85(2012)255–263.

[17] N. A.S. Al–Areqi, S. Beg, A. Al–Alas, Study on phase stability and oxide ion conductivity in the BIAGVOX system, *Journal of Physics and Chemistry of Solids* 73 (2012) 730–734.

[18] S. Beg, N. A.S. Al–Areqi, Kh.A.S. Ghaleb, A. Al–Alas, S. Hafeez, Effect of Ni(II) substitution on phase stabilization electrical properties of BICo(III)VOX.20 oxide–ion conductor, *Philosophical Magazine* 94(2014)1661–1673.

[19] A.E.H. Machado, J.A. de Miranda, R.F. de Freitas, E.T.F.M. Duarte, L.F. Ferreira, Y.D.T. Albuquerque, R. Ruggiero, C. Sattler, L. de Oliveira, Destruction of the organic matter present in effluent from a cellulose and paper industry using photocatalysis, *Journal of Photochemistry and Photobiology A: Chemistry* 155 (2003) 231–241.

[20] C.G. da Silva, J.L. Faria, Photochemical and photocatalytic degradation of an azo dye in aqueous solution by UV irradiation, *Journal of Photochemistry and Photobiology A: Chemistry* 155 (2003) 133–143.

[21] F. Krok, I. Abrahams , A. Zadrozna, M. Małys, W. Bogusz, J.A.G. Nelstrop, A.J. Bush, Electrical conductivity and structure correlation in BIZNVOX, *Solid State Ionics* 119 (1999) 139–144.

[22] N.A.S. Al–Areqi, S. Beg, Phase transition changes in $Bi_4Ce_xV_{2-x}O_{11-(x/2)-\delta}$ system, *Materials Chemistry Physics* 115 (2009) 5–8.

[23] R.D. Shannon and C.T. Prewitt, Effective ionic radii in oxides and fluorides, *Acta Crystallography B* 25 (1969) 925–946.

[24] E. Pernot, M. Anne, M. Bacmann, P. Strobe1, J. Fouletier, R.N. Vannier, G. Mairesse, F. Abraham, G. Nowogrocki, Structure and conductivity of Cu and Ni–substituted $Bi_2V_2O_{1\ 1}$ compounds, *Solid State Ionics* 70–71 (1994) 259–263.

[25] M. Alga, A. Ammar, R. Essalim, B. Tanouti, A. Outzourhit, F. Mauvy, R. Decourt, Study on structural, thermal, sintering and conductivity of Cu–Co doubly substituted $Bi_4V_2O_{11}$, *Ionics* 11 (2005)81–86.

[26] A. Watanabe , K. Das, Time–dependent degradation due to the gradual phase change in BICUVOX and BICOVOX oxide–ion conductors at temperatures below about 500°C, *J. Solid State Chemistry* 163 (2002) 224–230.

[27] W. Wrobel, I. Abrahams, F. Krok, A. Kozanecka, M. Malys, W. Bogusz, J.R. Dygas, Phase stabilization and electrical characterisation in the pseudo–binary system Bi_2ZrO_5–$Bi_2VO_{5.5-\delta}$, *Solid State Ionics* 175 (2004) 425–429.

[28] X. Yang, F. Ma, K. Li, Y. Guo, J. Hu, W. Li, M. Huo, Y. Guo, Mixed phase titania nanocomposite codoped with metallic silver and vanadium oxide: New efficient photocatalyst for dye degradation, *Journal of Hazardous Materials* 175 (2010) 429–438.

[29] I. Abrahams, F. Krok, Defect chemistry in the BIMEVOXes, *Journal of Materials Chemistry*12(2002)3351–3362.

[30] S. Beg, A. Al–Alas, N.A.S. Al–Areqi, Layered Aurivillius compound: Synthesis, characterization and electrical properties, *Journal of Alloys and Compounds* 504 (2010) 413–419.

[31] N.S.A. Al–Areqi, S. Beg, A. Al–Alas, Study on phase stability and oxide ion conductivity in the BIAGVOX system, *Journal of Physics and Chemistry of Solids* 73(2012)730–734.

[32] H. R. Pouretedal, M. H. Keshavarz, Synthesis and characterization of $Zn_{1-x}Cu_xS$ and $Zn_{1-x}Ni_xS$ nanoparticles and their applications as photocatalyst in Congo red degradation, *Journal of Alloys and Compounds* 501 (2010) 130–135.